Published on 11 April 2016. Downloaded by Beijing Institute of Nanoenergy and Nanosystems CAS on 31/05/2016 02:39:15.

Journal of Materials Chemistry C

PAPER

View Article Online
View Journal | View Issue

Cite this: J. Mater. Chem. C, 2016, 4, 4733

CuS nanotrough-networks for highly stable transparent conducting electrodes†

Xiaojia Zhang,‡[a] Wenxi Guo,‡[ab] Guoyun Gao,[a] Miaoling Que,[a] Caofeng Pan*[a] and Zhong Lin Wang*[a]

Received 9th March 2016,
Accepted 11th April 2016

DOI: 10.1039/c6tc01010e

www.rsc.org/MaterialsC

Here, we present a newly designed, highly flexible transparent conductive electrode based on a copper sulfide nanotrough network (CuS NN) film. This electrode achieves the sheet resistance of ~20 Ω sq^{-1} with a transmittance of up to 80%, which is produced by a process involving electrospinning, metal deposition and low temperature solvothermal reaction. The novel CuS NN film shows excellent chemical stability, exposed to various conditions of thermal oxidation at 160 °C, humid air with 80% relative humidity at 85 °C, and H_2O_2 solution, respectively. During the bending test, the CuS NN electrode exhibited remarkable mechanical stability. We have finished the four wire resistive touch-screen devices based on the CuS NN electrode, which illustrate a promising alternative to traditional TCE materials for wearable electronic devices.

Introduction

Highly transparent conducting electrodes (TCEs) based on indium tin oxide (ITO) have attracted great attention due to their applications in optoelectronic devices such as e-readers, touch screens, smart-glass, solar cells, displays and organic light emitting diodes (OLEDs).[1–4] However, the scarcity, poor mechanical flexibility, low optical transmittance and high processing temperature of indium limit its applications in stretchable electronics.[5–10] As for the alternatives to ITO, graphene, carbon nanotubes (CNTs), conducting polymers and metal nanowires/nanotroughs have been studied.[11–27] Graphene TCEs with excellent electrical and optical properties can be fabricated by chemical vapor deposition (CVD) and the "roll to roll" transfer process, but a high temperature CVD process is not practical for production of a low-cost alternative to ITO.[12–15,28] Although CNTs demonstrate better flexibility and durability, their relatively poor conductivity (~60–400 Ω sq^{-1} at 90% transmittance) limits their application in optoelectronic devices.[17,29] Conducting polymers, *e.g.* poly(3,4-ethylenedioxythiophene)poly-(styrenesulfonate) (PEDOT:PSS), cannot match the same performance as ITO at low sheet resistance (less than 100 Ω sq^{-1}).[22,23,25,26] Metal nanowires/nanotroughs, such as Ag and Cu, exhibit excellent electrical and optical properties, which are promising alternatives to traditional transparent ITO electrodes.[16–18,20–25,29–31]

Given that Cu is ~1000 times more abundant and ~100 times cheaper than Ag or indium,[21,31] Cu nanowire/nanotrough TCEs have attracted considerable attention as potential alternatives to Ag nanowire TCEs. Due to their poor stability, Cu nanowires/nanotroughs are prone to oxidation even when exposed to air at room temperature. Many approaches have been searched to solve the stability of Cu nanowires/nanotroughs, such as a polymer protection layer, a aluminum-doped zinc oxide/aluminum oxide protection layer, a nickel shell protection layer and a graphene shell protection layer.[12,27,31–36] However, the whole process of fabricating these protection layers is complicated, and costly techniques such as atomic layer deposition (ALD) or plasma enhanced chemical vapor deposition (PECVD) are introduced. Therefore, the challenge still remains to search for a cost-effective facile method to develop new stable TCEs.

Herein, we construct a highly transparent conductive CuS NN electrode on different flexible substrates at low temperature. The novel CuS NN electrode obtained the sheet resistance of 20 Ω sq^{-1} (T > 80%), which is much better than the previous reported CuS TCE.[37–39] In addition, we further demonstrate that the novel CuS NN TCE is highly resistant to oxidation and has remarkable mechanical flexibility. A flexible touch-screen was successfully demonstrated for the first time by using a CuS NN TCE. We anticipate that the novel CuS NN electrode can be used in optoelectronic devices such as flexible solar cells, touch screen panels and organic light-emitting diodes.

Results and discussion

The fabrication process of CuS NN electrodes can be divided into two steps as shown in Fig. 1a–e. First of all, Cu NNs were constructed on flexible substrates by electrospinning and

[a] Beijing Institute of Nanoenergy and Nanosystems, Chinese Academy of Sciences; National Center for Nanoscience and Technology (NCNST), Beijing, 100083, P. R. China. E-mail: cfpan@binn.cas.cn
[b] Research Institution for Biomimetics and Soft Matter and Department of Physics, Xiamen University, Xiamen, 361005, P. R. China. E-mail: wxguo@xmu.edu.cn

† Electronic supplementary information (ESI) available: Videos 1, 2 and 3, and SEM images. See DOI: 10.1039/c6tc01010e

‡ These authors contributed equally to this work.

Published on 11 April 2016. Downloaded by Beijing Institute of Nanoenergy and Nanosystems CAS on 31/05/2016 02:39:15.

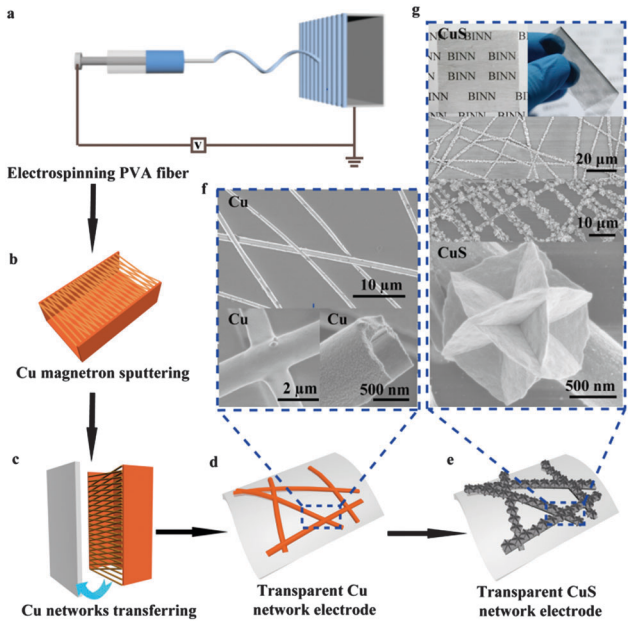

Fig. 1 Schematic illustration of the fabrication processes of the CuS NN electrode. (a) PVA fiber was assembled in networks on an aluminum frame by electrospinning; (b) Cu nanoparticles were deposited on the PVA surface by magnetron sputtering or the thermal evaporation method; (c) the Cu NNs were transferred to the PET substrate and the PVA core was dissolved away; (d) the Cu NN electrode was obtained; (e) Cu NNs were converted into CuS NNs by sulfur treatment; (f) the SEM images of the Cu NN electrodes; (g) the optical and SEM images of the as-fabricated CuS NN electrodes.

magnetron sputtering as previously reported by Cui *et al.*[21] Free-standing and long poly(vinyl alcohol) (PVA) nanofiber networks were collected by an aluminum (Al) foil frame using electrospinning (Fig. 1a). After a thin layer of copper (Cu) was deposited on the PVA networks using magnetron sputtering as shown in Fig. 1b, the metallized fibers were transferred to an arbitrary flexible substrate (plastics, paper or rubber) and the Cu NNs were derived after removing the PVA nanofibers from deionized water as shown in Fig. 1c and d. The SEM images of the obtained Cu NNs are shown in Fig. 1f; it is obvious that the Cu nanotroughs have a half-shell cross-section and are interconnected with each other without cracks. The transparency and the conductivity of the Cu NN electrodes can be easily controlled by the density of the Cu nanotroughs. The nanotroughs can attach on the PET substrates firmly even when we tried to peel them off with Kapton tape, which can be seen in the ESI,† Movie S1.

Secondly, the obtained Cu NNs were immersed in ethanol containing excessive sulfur powders at 60 °C for several hours. It is obvious from the photographs in Fig. 1g that the color of the Cu NNs on the PET substrates gradually changed to neutral-gray as presented in Fig. 1e. The corresponding scanning electron microscopy (SEM) images as shown in Fig. 1g with different magnifications reveal that the Cu NNs were transformed into dense CuS nanoflowers consisting of nanosheets (NSs) after 12 h sulphur treatment. The SEM images of the CuS NNs with different densities are shown in Fig. S1, ESI†, and different densities of CuS NNs lead to different sheet resistances from 1 to 50 Ω sq^{-1}. Compared to other transparent conducting electrodes (TCEs), our CuS NNs have excellent transparency, perfect conductivity and relatively low cost (Fig. S2, ESI†).[40–63] Besides that, the CuS NN electrodes can achieve equivalent performance to ITO (Table S1, ESI†).

To investigate the component and structure of the CuS NNs, X-ray diffraction (XRD), Raman spectroscopy and transmission electron microscopy (TEM) were performed as shown in Fig. 2, respectively. Fig. 2a displays the XRD spectra of Cu NNs before and after 12 h sulphur treatment. The diffraction peaks in red color, located at 27.6°, 29.3°, 31.8°, 48.1°, and 59.2°, can be readily indexed to (101), (102), (103), (110), and (116) of a pure hexagonal CuS phase, according to the Joint Committee on Powder Diffraction Standards (JCPDS card no. 06-0464). And the sharp diffraction peaks imply that the prepared CuS NNs were well crystallized. The Raman spectrum displayed in Fig. 2b exhibits a very sharp peak at 471 cm^{-1} due to S–S stretching, which can be attributed to the lattice vibrations of CuS. Furthermore, the crystal structure of a CuS NN was analyzed by TEM and high-resolution transmission electron microscopy (HRTEM) as shown in Fig. 2c. The lattice spacing of 0.314 nm as marked in Fig. 2c matches well with the interplanar spacing (101) planes of the hexagonal CuS phase and indicates that the CuS nanosheet grows along the [101] crystallographic direction. Furthermore, the corresponding selected area electron diffraction (SAED)

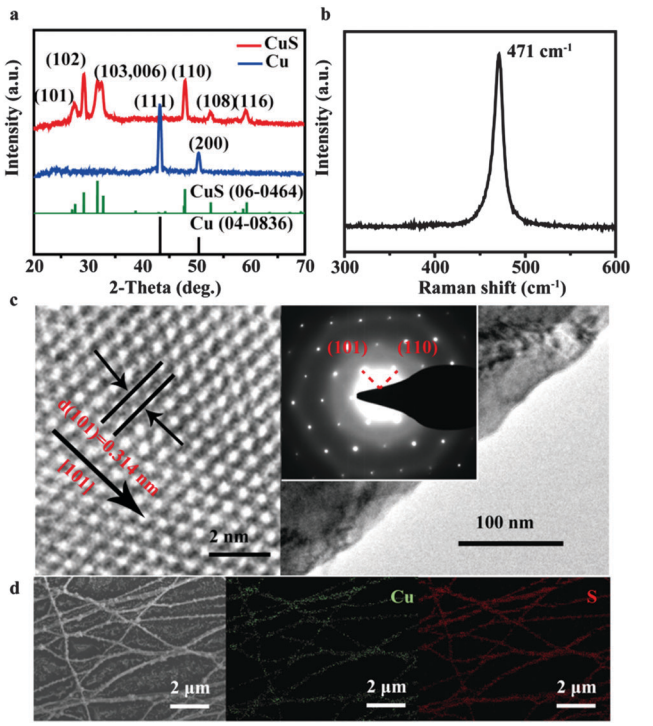

Fig. 2 Characterization of the CuS NN electrodes. (a) XRD spectra of the Cu and CuS NN electrodes; (b) Raman spectra of CuS NN electrodes; (c) the transmission electron microscopy (TEM) image, the high-resolution transmission electron microscopy (HRTEM) image and the selected area electron diffraction (SAED) pattern of the CuS NN electrodes; (d) EDS mapping images of the as-fabricated CuS NN.

 This journal is © The Royal Society of Chemistry 2016

Published on 11 April 2016. Downloaded by Beijing Institute of Nanoenergy and Nanosystems CAS on 31/05/2016 02:39:15.

pattern obtained from the red area in Fig. 2c shows several diffraction points, which can be indexed to the (101) and (011) lattice planes of the hexagonal phase of CuS as well. The CuS NNs were further investigated by elemental analysis *via* energy dispersive X-ray spectroscopy (EDX) (Fig. S3, ESI†) indicating that the CuS nanosheets consist of only Cu and S. The corresponding EDX mapping in Fig. 2d shows that Cu and S elements are uniformly distributed on the whole networks, indicating that most of the Cu NNs were converted into CuS NNs after 12 h sulphur treatment. The variation tendency of the sheet resistance of Cu NNs with increasing sulphur treatment time is shown in Fig. 3. Fig. 3a(A–E) shows the XRD patterns of the Cu NNs upon reaction with sulphur for 20 min, 60 min, 80 min, 6 h and 3 days, respectively. The corresponding SEM images of different reaction times are displayed in Fig. 3b. The formation mechanism of the CuS NNs can be attributed to a typical Ostwald ripening process.[64] At the very beginning, the sulfur powders in ethanol can easily permeate into the sputtered Cu film and react with the Cu nanotroughs. After 20 min reaction, some flower-like CuS architectures appeared, scattered on the surface of Cu nanotroughs as shown in Fig. 3b-A3. The corresponding XRD pattern indicates that the emergence of some tiny diffraction peaks can be readily indexed to (101), (102), (103), (110) and (116) of a pure hexagonal CuS phase. These flower-like CuS architectures served as the seeds to guide the subsequent growth of CuS NNs, and once the nucleus forms on the nanotrough, the growth speed increases rapidly and abundant nanosheets completely spread across the network as time was increased to 60–80 min which could be observed in Fig. 3b-B and 3b-C. As the reaction time increases, the corresponding XRD patterns show the obviously increased CuS diffraction peaks and decreased Cu diffraction peaks. When the growth time was extended to more than 6 h, dense CuS NNs were formed and the diffraction peaks for Cu disappeared. No obvious changes were observed in the XRD pattern and SEM images when we further increased the reaction time to 3 days, indicating that all the Cu nanotroughs were converted into CuS.

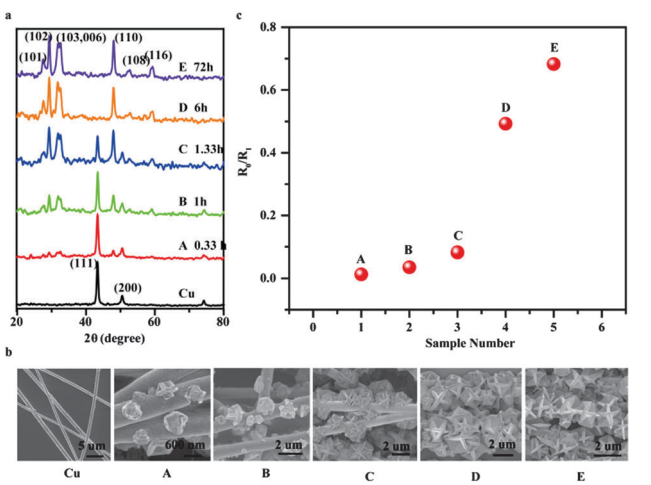

Fig. 3 The variation tendency of Cu NNs with different sulphur treatment times. (a) XRD patterns of the Cu NN upon reaction with sulphur for 20 min, 60 min, 80 min, 6 h and 3 days, respectively; (b) the corresponding SEM images are displayed on the right; (c) the variation trend of the normalized sheet resistance (R_0/R_1) of Cu NNs as a function of reaction time.

It is worth noting that the sulphur treatment time will greatly affect the conductivity of the Cu NNs. At the beginning, the sheet resistance of the film increased sharply and reached its minimum value (R_0/R_1 = 0.012) when the reaction time was 20 min as shown in Fig. 3c. Interestingly, the sheet resistance decreased when we further increased the immersion time and finally reached a stable value $R_0/R_1 \approx 0.7$, which is close to the sheet resistance of the Cu NNs. This phenomenon may be explained as follows: the initial sharp increase of the sheet resistance of the Cu NN film was due to the fact that Cu is prone to react with sulphur and forms a poor conductive CuS passivation layer. Upon increasing the reaction time, monocrystalline covellite CuS, which is known to be an excellent p-type conducting material, provided conduction holes to decrease the sheet resistance. The sheet resistances were further decreased and reached a stable minimum value until all the Cu NNs were converted into CuS.

To investigate the variations of the transmittance and sheet resistance for Cu and CuS NNs as a function of reaction time, ten Cu NN films were immersed in sulphur ethanol solution for over 24 h and the normalized sheet resistance (R_1/R_0) and transmittance (T_1/T_0) were obtained (Fig. S4, ESI†). Only ~5% average degradation in transmittance was observed at the wavelength of 550 nm while 150–200% average increase in sheet resistance was observed when Cu NNs were converted into CuS NNs. Fig. S5 (in the ESI†) indicates the variation tendency of transmittance upon increasing the sheet resistance of CuS NNs on PET at 550 nm wavelength. The transmittance of CuS NN electrodes increased upon increasing the sheet resistance of CuS NNs; over 80% optical transmittance was achieved with the sheet resistances less than 20 Ω sq^{-1}. Compared to the previous results on CuS TCEs,[37–39] our CuS NN TCEs show a superb level of transparency and sheet resistance. Transparency is very important for TCEs. Fig. 4a displays the transmittance spectra of the Cu and CuS NN electrodes, commercial FTO/glass and ITO/glass electrodes from 400 to 2000 nm. Both the Cu and CuS NN electrodes demonstrated high transmittance from the visible to the near-infrared light and present a flat spectrum for the entire wavelength range from 400 to 2000 nm while the transmittances of commercial FTO/glass and ITO/glass electrodes demonstrated a sharp decrease in the transmittance spectra in the near-infrared wavelength range from 1000 nm to 2000 nm. The superior transparency of the novel electrode would be used in near-infrared sensors and detectors. Chemical stability is another important feature of TCEs. Cu nanotrough/nanowire TCEs are promising next-generation transparent electrodes replacing ITO, which are easy to oxidize, and the oxidation would hinder wide application. Fig. 4b and c show thermostability tests for Cu and CuS NNs by measuring the variation trend of sheet resistance at 85 °C in humid air with 80% relative humidity and at 160 °C in the oven, respectively. The sheet resistance of the CuS NN film remained remarkably stable over a period of 16 days when the temperature was 85 °C in humid

Published on 11 April 2016. Downloaded by Beijing Institute of Nanoenergy and Nanosystems CAS on 31/05/2016 02:39:15.

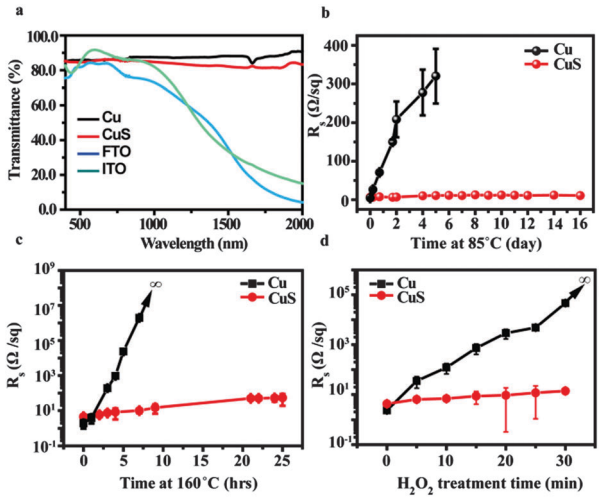

Fig. 4 Transmittance and chemical stability tests for CuS NN electrodes. (a) Transmittance spectra of the as-prepared network electrodes and commercialized transparent conductive film (ITO and FTO on glass) scanned from 400 nm to 2000 nm; (b) and (c) the variation trend of the sheet resistance of Cu and CuS NN as function of the baking time in the humid air with 80% relative humidity at 85 °C and in the oven at 160 °C, respectively; (d) the variation trend of the sheet resistance of the Cu and CuS NN as function of the H_2O_2 treatment time.

air with 80% relative humidity, while the sheet resistance of the Cu electrode increased by an order of magnitude. Similarly, the sheet resistance of the CuS NN film still remained relatively stable when the temperature was 160 °C, but the sheet resistance of the Cu NN electrode increased dramatically and it became insulating (more than 106 Ω sq^{-1}) after merely 7 h of exposure. A color change from reddish orange to gray yellow due to the conversion of Cu to CuO is accompanied by a sharp increase of sheet resistance (Fig. S6, ESI†). Unlike the Cu NN film, the CuS NN film retained the original color during the whole exposure. Furthermore, both the network films were tested in H_2O_2 (2 wt%) solution and similar results were obtained as shown in Fig. 4d. There was only a slight increase in the sheet resistance of the CuS NN electrode even when the treatment time was extended to 35 min. In contrast, the sheet resistance of Cu NN electrodes increased dramatically and they became insulating after 30 minute treatment. We immerse the bare Cu and the CuS NN electrode into aqueous solution with different pH values for 1 min to test the corrosion resistance of the CuS nanotroughs (Fig. S7, ESI†). In the solutions of different pH values, no obvious change in the resistance of the CuS NN electrode was observed, indicating remarkable resistance against corrosion. However, the poor Cu NN electrode suffers from severe itching in acidic solutions due to its inferior chemical stability, and the sheet resistance increased sharply.

The mechanical stability of the CuS NN electrode was further tested under twisting deformation and cyclic bending. Fig. 5a and b illustrate the minimum and maximum bending deformation of the CuS NN on a 2 cm × 2 cm PET substrate. To examine mechanical durability, the electrode was bent to the radius of 0.25 cm and 0.5 cm, and then released to the

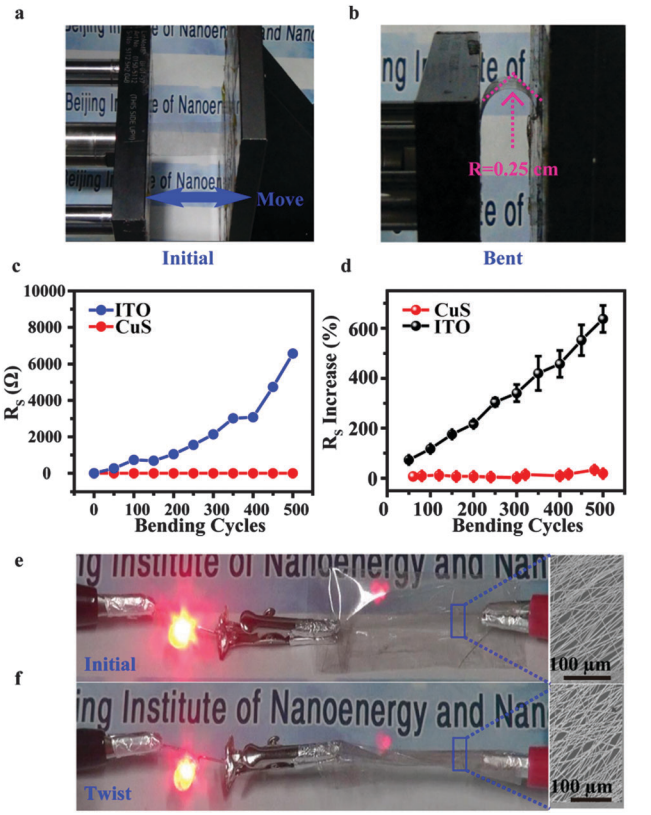

Fig. 5 The mechanical stability tests for CuS NN TCEs. (a) and (b) The photographic images of the experimental setup for the bending test; bending radius are 0.25 cm and 0.5 cm, respectively; The variations in resistance of a CuS NN electrode and an ITO electrode on PET film as a function of the number of bending cycles at the bending radius of (c) 0.25 cm and (d) 0.5 cm, respectively; (e) and (f) are photographic images of working LED with releasing and twisting CuS NN electrodes as segments of external circuits; the right part are the corresponding SEM images of CuS NN film before and after 500 time twisting tests, respectively.

initial position, repetitively 500 times. The resistance of the CuS NN electrode and the commercial ITO/PET electrode as a function of the number of bending cycles is shown in Fig. 5c and d. It was obvious that the percentage of the sheet resistance increase of the commercial ITO/PET electrode dramatically increased due to the brittleness of the film, while negligible changes in the resistance were observed for CuS NNs with the bending radii of 0.25 cm and 0.5 cm. Fig. 5e and f show the photographic images of the working LED connected with releasing and twisting CuS NN electrodes as segments of external circuits; the right part shows the corresponding SEM images of the CuS NN film before and after the twisting test at the angle of 720°, respectively. The real-time working states of the LED and the whole operations described above are recorded in the ESI,† Movie S2. No obvious change in the brightness of the LED was observed from the movie. Furthermore, there were no cracks observed on the surface from SEM images on the right part after twisting the angle by 720°. This superior mechanical strength is attributed to the strong adhesion of the CuS nanotroughs to the PET substrate and the inherent resilience of the CuS nanotroughs. Moreover, surface tension of the CuS nanosheet film

 This journal is © The Royal Society of Chemistry 2016

Published on 11 April 2016. Downloaded by Beijing Institute of Nanoenergy and Nanosystems CAS on 31/05/2016 02:39:15.

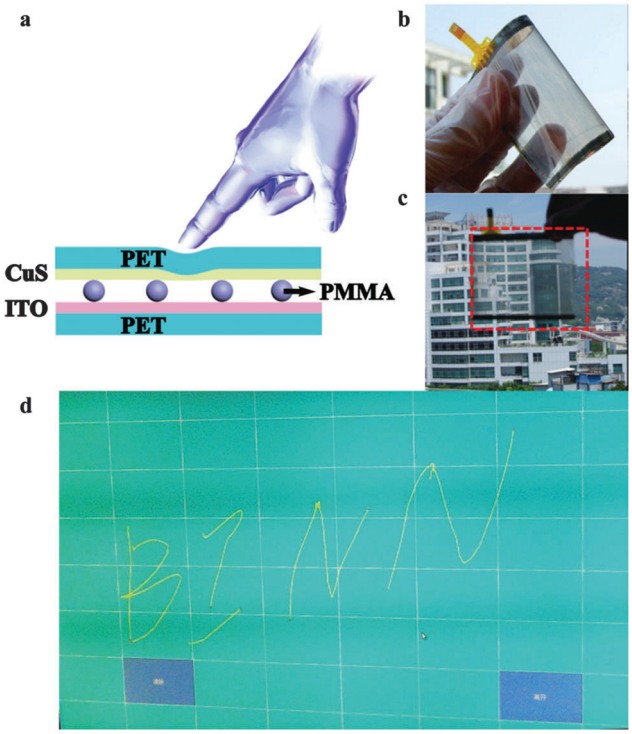

Fig. 6 High performance touch panel based on CuS NN TCEs. (a) The scheme of the structure of the resistance 4-line touch panel; (b) and (c) are the photographs of as-fabricated flexible resistive touch-screen device based on CuS NN TCEs; (d) video clips of the touch screen operation fabricated by CuS NN TCEs. A word "BINN" was written on the touch panel.

on nanotroughs is much smaller than that on a flexible flat substrate as reported previously. In comparison, CuS nanosheets were also synthesized on Cu/PET in the same way. The CuS nanosheet film that cracked and detached from the PET substrate went through several cycles, indicating that the nanotrough CuS structure networks have much better mechanical durability than the continuous CuS film on flexible substrates (Fig. S8, ESI†). The excellent electrical stability and the superior flexibility of the CuS NN electrodes would extend their potential applications to flexible solar cells and touch screens or organic light emitting diodes. Herein, as shown in Fig. 6, we have integrated our CuS NN electrode into a flexible resistive touch-screen device; it is demonstrated in the Movie S3 (in the ESI†). The typical structure of the resistance 4-line touch panel fabricated with the CuS NN is shown in Fig. 6a, and the photographs of the whole touch panel are shown in Fig. 6b and c. The device worked well when we wrote "BINN" on it, as shown in Fig. 6d.

Conclusions

In summary, a newly designed CuS NN TCE with high transparency, flexibility and conductivity has been developed by a process involving electrospinning, metal deposition and a low temperature solvothermal reaction. The novel conducting film exhibits remarkable mechanical properties during the bending and twisting tests. Its synthesis is facile and amenable to scale up based on standard electrospinning and metal deposition techniques. In addition, CuS NNs showed excellent chemical stability at high temperature, in H_2O_2 and various pH value tests, indicating that such network electrodes could replace ITO, which can be widely used in solar cells, touch sensors and flat panel displays, and could find use in emerging application areas such as flexible electronics and skin-like sensors.

Experimental

CuS NN film fabrication

First of all, the transparent Cu NNs were fabricated on polymer substrates using electrospinning and sputtering methods as reported previously: free-standing PVA fibers were spun on an aluminum frame to form a network and then a thin layer of Cu film with a thickness of 50–100 nm was deposited on the polymer fiber network by sputtering. The Cu NNs were derived after transferring the whole structure onto the polymer substrate and removing the PVA nanofibers. Second, CuS nanosheets were fabricated on the Cu NNs by sulfur deposition. The as-fabricated Cu NN electrodes were converted into CuS nanosheet networks by soaking them in sulfur ethanol solution (0.01 M) at 60 °C for 6–24 h.

The fabrication of touch screen devices

A four-wire analogue-resistive touch-screen device was fabricated as follows: First, a 2.8 inch CuS NN electrode on a PET film as the top layer and a same size piece of the traditional ITO electrode as the bottom layer were selected. Second, these two electrodes were printed using silver ink for signal pin out. Third, we printed PMMA dot spacers on the ITO electrode and attached the bottom and the top layers. At last, we bounded the pin out circuit. The whole process was the same as the ITO-based touch screen panel. Testing software was provided by TVI Electronics.

Characterization

A digital multimeter (Keithley 2100) with a four-point probe was used to measure the sheet resistances of the films. The light transmittance of the hybridized electrodes was measured by UV-vis spectroscopy (Shimadzu UV-3600). The optical images were taken by using a Canon digital camera. The morphology and structure of the prepared hybridized electrodes were examined by scanning electron microscopy (SEM, Hitach 8000) and transmission electron microscopy (TEM, F20). The phase identification of the hybridized electrodes was conducted by X-ray diffraction (XRD) using a PANalytical X'Pert PRO diffractometer.

Acknowledgements

The authors are thankful for support from the "Thousand Talents" program of China for pioneering researchers and innovative teams and from the President Funding of the Chinese Academy of Sciences, National Natural Science Foundation of China

Published on 11 April 2016. Downloaded by Beijing Institute of Nanoenergy and Nanosystems CAS on 31/05/2016 02:39:15.

(No. 51432005, 61405040, 61505010 and 51502018), Beijing City Committee of science and technology (Z151100003315010), Beijing Natural Science Foundation (2164077 and 2164076).

Notes and references

1 H. Liu, V. Avrutin, N. Izyumskaya, Ü. OzgUr and H. Morkoç, *Superlattices Microstruct.*, 2010, **48**, 458–484.
2 D. S. Ginley, H. Hosono and D. C. Paine, *Handbook of Transparent Conductors*, 2010.
3 B. G. Lewis and D. C. Paine, *MRS Bull.*, 2000, **25**, 22–27.
4 T. Minami, *Semicond. Sci. Technol.*, 2005, **20**, S35–S44.
5 Z. Chen, B. Cotterell and W. Wang, *Eng. Fract. Mech.*, 2002, **69**, 597–603.
6 D. R. Cairns, R. P. Witte, D. K. Sparacin, S. M. Sachsman, D. C. Paine, G. P. Crawford and R. R. Newton, *Appl. Phys. Lett.*, 2000, **76**, 1425–1427.
7 J. Lewis, *Mater. Today*, 2006, **9**, 38–45.
8 Y. Leterrier, L. Medico, F. Demarco, J. A. E. Manson, U. Betz, M. F. Escola, M. Kharrazi Olsson and F. Atamny, *Thin Solid Films*, 2004, **460**, 156–166.
9 Z. Chen, B. Cotterell, W. Wang, E. Guenther and S. J. Chua, *Thin Solid Films*, 2001, **394**, 202–206.
10 B. W. An, B. G. Hyun, S. Y. Kim, M. Kim, M. S. Lee, K. Lee, J. B. Koo, H. Y. Chu, B. S. Bae and J. U. Park, *Nano Lett.*, 2014, **14**, 6322–6328.
11 L. Zhou, H. Y. Xiang, S. Shen, Y. Q. Li, J. De Chen, H. J. Xie, I. A. Goldthorpe, L. S. Chen, S. T. Lee and J. X. Tang, *ACS Nano*, 2014, **8**, 12796–12805.
12 Y. Ahn, Y. Jeong, D. Lee and Y. Lee, *ACS Nano*, 2015, **9**, 3125–3133.
13 K. S. Kim, Y. Zhao, H. Jang, S. Y. Lee, J. M. Kim, K. S. Kim, J. H. Ahn, P. Kim, J. Y. Choi and B. H. Hong, *Nature*, 2009, **457**, 706–710.
14 N. O. Weiss, H. L. Zhou, L. Liao, Y. Liu, S. Jiang, Y. Huang and X. F. Duan, *Adv. Mater.*, 2012, **24**, 5782–5825.
15 S. Bae, H. Kim, Y. Lee, X. F. Xu, J. S. Park, Y. Zheng, J. Balakrishnan, T. Lei, H. R. Kim, Y. I. Song, Y. J. Kim, K. S. Kim, B. Ozyilmaz, J. H. Ahn, B. H. Hong and S. Iijima, *Nat. Nanotechnol.*, 2010, **5**, 574–578.
16 D. S. Hecht, L. B. Hu and G. Irvin, *Adv. Mater.*, 2011, **23**, 1482–1513.
17 M. Zhang, S. L. Fang, A. A. Zakhidov, S. B. Lee, A. E. Aliev, C. D. Williams, K. R. Atkinson and R. H. Baughman, *Science*, 2005, **309**, 1215–1219.
18 S. De, T. M. Higgins, P. E. Lyons, E. M. Doherty, P. N. Nirmalraj, W. J. Blau, J. J. Boland and J. N. Coleman, *ACS Nano*, 2009, **3**, 1767–1774.
19 Z. Chen, S. Ye, I. E. Stewart and B. J. Wiley, *ACS Nano*, 2014, **8**, 9673–9679.
20 S. Soltanian, R. Rahmanian, B. Gholamkhass, N. M. Kiasari, F. Ko and P. Servati, *Adv. Energy Mater.*, 2013, **3**, 1332–1337.
21 H. Wu, D. S. Kong, Z. C. Ruan, P. C. Hsu, S. Wang, Z. F. Yu, T. J. Carney, L. B. Hu, S. H. Fan and Y. Cui, *Nat. Nanotechnol.*, 2013, **8**, 421–425.
22 J. Lee, P. Lee, H. B. Lee, S. Hong, I. Lee, J. Yeo, S. S. Lee, T. S. Kim, D. Lee and S. H. Ko, *Adv. Funct. Mater.*, 2013, **23**, 4171–4176.
23 W. Gaynor, G. F. Burkhard, M. D. McGehee and P. Peumans, *Adv. Mater.*, 2011, **23**, 2905–2910.
24 F. Xu and Y. Zhu, *Adv. Mater.*, 2012, **24**, 5117–5122.
25 S. Yun, X. F. Niu, Z. B. Yu, W. L. Hu, P. Brochu and Q. B. Pei, *Adv. Mater.*, 2012, **24**, 1321–1327.
26 S. Kirchmeyer and K. Reuter, *J. Mater. Chem.*, 2005, **15**, 2077.
27 P. C. Hsu, H. Wu, T. J. Carney, M. T. McDowell, Y. Yang, E. C. Garnett, M. Li, L. B. Hu and Y. Cui, *ACS Nano*, 2012, **6**, 5150–5156.
28 D. S. Hecht, L. Hu and G. Irvin, *Adv. Mater.*, 2011, **23**, 1482–1513.
29 S. R. Ye, A. R. Rathmell, Z. F. Chen, I. E. Stewart and B. J. Wiley, *Adv. Mater.*, 2014, **26**, 6670–6687.
30 K. Ellmer, *Nat. Photonics*, 2012, **6**, 808–816.
31 Z. F. Chen, S. R. Ye, I. E. Stewart and B. J. Wiley, *ACS Nano*, 2014, **8**, 9673–9679.
32 I. E. Stewart, A. R. Rathmell, L. Yan, S. R. Ye, P. F. Flowers, W. You and B. J. Wiley, *Nanoscale*, 2014, **6**, 5980–5988.
33 J. Y. Chen, W. X. Zhou, J. Chen, Y. Fan, Z. Q. Zhang, Z. D. Huang, X. M. Feng, B. X. Mi, Y. W. Ma and W. Huang, *Nano Res.*, 2015, **8**, 1017–1025.
34 A. R. Rathmell, M. Nguyen, M. Chi and B. J. Wiley, *Nano Lett.*, 2012, **12**, 3193–3199.
35 S. Kiruthika, R. Gupta, A. Anand, A. Kumar and G. U. Kulkarni, *ACS Appl. Mater. Interfaces*, 2015, **7**, 27215–27222.
36 S. Kiruthika, R. Gupta, K. D. M. Rao, S. Chakraborty, N. Padmavathy and G. U. Kulkarni, *J. Mater. Chem. C*, 2014, **2**, 2089.
37 K. D. Yuan, J. J. Wu, M. L. Liu, L. L. Zhang, F. F. Xu, L. D. Chen and F. Q. Huang, *Appl. Phys. Lett.*, 2008, **93**, 1332106.
38 A. Cuevas, R. Romero, D. Leinen, E. A. Dalchiele, J. R. Ramos-Barrado and F. Martin, *Sol. Energy Mater. Sol. Cells*, 2015, **134**, 199–208.
39 S. Erokhina, V. Erokhin and C. Nicolini, *Langmuir*, 2003, **19**, 766–771.
40 B. Dan, G. C. Irvin and M. Pasquali, *ACS Nano*, 2009, **3**, 835–843.
41 G. Eda, G. Fanchini and M. Chhowalla, *Nat. Nanotechnol.*, 2008, **3**, 270–274.
42 A. Elschner and W. Lövenich, *MRS Bull.*, 2011, **36**, 794–798.
43 B. Friedel, T. J. K. Brenner, C. R. McNeill, U. Steiner and N. C. Greenham, *Org. Electron.*, 2011, **12**, 1736–1745.
44 W. He and C. Ye, *J. Mater. Sci. Technol.*, 2015, **31**, 581–588.
45 H. A. Becerril, J. Mao, Z. Liu, R. M. Stoltenberg, Z. Bao and Y. Chen, *ACS Nano*, 2008, **2**, 463–470.
46 A. A. Green and M. C. Hersam, *Nano Lett.*, 2008, **8**, 1417–1422.
47 H.-Z. Geng, K. K. Kim, K. P. So, Y. S. Lee, Y. Chang and Y. H. Lee, *J. Am. Chem. Soc.*, 2007, **129**, 7758–7759.
48 Z. Hu, J. Zhang and Y. Zhu, *Renewable Energy*, 2014, **62**, 100–105.
49 M. Kaempgen, G. S. Duesberg and S. Roth, *Appl. Surf. Sci.*, 2005, **252**, 425–429.

 This journal is © The Royal Society of Chemistry 2016

Published on 11 April 2016. Downloaded by Beijing Institute of Nanoenergy and Nanosystems CAS on 31/05/2016 02:39:15.

50 J. Lee, P. Lee, H. Lee, D. Lee, S. S. Lee and S. H. Ko, *Nanoscale*, 2012, **4**, 6408–6414.
51 L. Hu, H. S. Kim, J.-Y. Lee, P. Peumans and Y. Cui, *ACS Nano*, 2010, **4**, 2955–2963.
52 S.-I. Na, S.-S. Kim, J. Jo and D.-Y. Kim, *Adv. Mater.*, 2008, **20**, 4061–4067.
53 B. B. Parekh, G. Fanchini, G. Eda and M. Chhowalla, *Appl. Phys. Lett.*, 2007, **90**, 121913.
54 P. Blake, P. D. Brimicombe, R. R. Nair, T. J. Booth, D. Jiang, F. Schedin, L. A. Ponomarenko, S. V. Morozov, H. F. Gleeson, E. W. Hill, A. K. Geim and K. S. Novoselov, *Nano Lett.*, 2008, **8**, 1704–1708.
55 A. R. Rathmell, S. M. Bergin, Y. L. Hua, Z. Y. Li and B. J. Wiley, *Adv. Mater.*, 2010, **22**, 3558–3563.
56 A. R. Rathmell and B. J. Wiley, *Adv. Mater.*, 2011, **23**, 4798–4803.
57 S.-Y. Bae, I.-Y. Jeon, J. Yang, N. Park, H. S. Shin, S. Park, R. S. Ruoff, L. Dai and J.-B. Baek, *ACS Nano*, 2011, **5**, 4974–4980.
58 S. De, T. M. Higgins, P. E. Lyons, E. M. Doherty, P. N. Nirmalraj, W. J. Blau, J. J. Boland and J. N. Coleman, *ACS Nano*, 2009, **3**, 1767–1774.
59 V. C. Tung, L.-M. Chen, M. J. Allen, J. K. Wassei, K. Nelson, R. B. Kaner and Y. Yang, *Nano Lett.*, 2009, **9**, 1949–1955.
60 R. L. Wang and H. B. Ruan, *J. Alloys Compd.*, 2016, **656**, 936–943.
61 H. Wu, L. Hu, M. W. Rowell, D. Kong, J. J. Cha, J. R. McDonough, J. Zhu, Y. Yang, M. D. McGehee and Y. Cui, *Nano Lett.*, 2010, **10**, 4242–4248.
62 S. Ye, A. R. Rathmell, I. E. Stewart, Y. C. Ha, A. R. Wilson, Z. Chen and B. J. Wiley, *Chem. Commun.*, 2014, **50**, 2562–2564.
63 Z. Yu, Q. Zhang, L. Li, Q. Chen, X. Niu, J. Liu and Q. Pei, *Adv. Mater.*, 2011, **23**, 664–668.
64 W. J. Ke, G. J. Fang, H. W. Lei, P. L. Qin, H. Tao, W. Zeng, J. Wang and X. Z. Zhao, *J. Power Sources*, 2014, **248**, 809–815.